

On-line monitoring of the keyhole welding pool in variable polarity plasma arc welding

H Wang and R Kovacevic*

Research Center for Advanced Manufacturing, Southern Methodist University, Richardson, Texas, USA

Abstract: This paper presents a technique to monitor the weld penetration in real time by the front-side image sensing of the keyhole welding pool in variable polarity plasma arc welding (VPPAW) of a 6061 aluminium alloy. A novel optical system is developed to acquire the keyhole welding pool images from two sides of the plasma arc welding torch. The geometric sizes of the visible keyhole can be accurately obtained by using the developed image-processing algorithm. The variation in sizes of the visible keyhole has a close relationship with the real diameter of the keyhole. An artificial neural network (ANN) model is established to describe the relationship between the keyhole diameter and the geometrical sizes of the keyhole welding pool obtained from the image.

Keywords: image sensing, keyhole welding pool, VPPAW

NOTATION

a_i	output of processing element i
a_{jn}	output of processing element jn
A	last point that can be detected along the Y direction on the keyhole edge of the left image
A'	perpendicular projection point of point A on the y axis in the image
B	intersection point of the XX' axis and the keyhole edge on the left image
C	last point that can be detected along the Y direction on the keyhole edge of the right image
C'	perpendicular projection point of point C on the y axis in the image
D	intersection point of the XX' axis and the keyhole edge on the right image
e	base index = 2.17828
$f(k, l)$	grey level of the pixel with the coordinate of row k and column l
$f(x)$	activation function ()
$g(i, j)$	enhanced grey level of the pixel (i, j)
in_i	weighted sum of the inputs to processing element i
K_{en}	factor of the direction enhancement operator
K_r	ratio of the standard local variance to the original variance

m_{av}	averaged grey level of the pixels included in the enhancement window
O ₁	central point of the keyhole on the left image
O ₂	central point of the keyhole on the right image
$w_{jn,i}$	link weight from processing element jn to processing element i
x_A, y_A	coordinate of point A
x_B, y_B	coordinate of point B
x_C, y_C	coordinate of point C
x_D, y_D	coordinate of point D

1 INTRODUCTION

In the late 1960s, B. Van Cleave, of the Boeing Company, combined the Sciaky variable polarity power source with the plasma keyhole technique and developed the variable polarity plasma arc welding (VPPAW) process. To achieve the desired welds, further development was required on the variable polarity power source. Hobart Brothers, under contract to Boeing in 1974, built a power supply that proved satisfactory. In 1978, NASA found that this important new process had the potential to replace gas tungsten arc welding (GTAW) for welding the aluminium fuel external tank on the Space Shuttle [1]. Many commercial products were developed for the space programme, and VPPAW was the first new welding process as a result from the programme. VPPAW features a combination of a direct current electrode negative (DCEN) period and a direct current electrode positive (DCEP) period in a cycle. Thus, it is an alternative current (AC) welding

The MS was received on 8 October 2001 and was accepted after revision for publication on 24 May 2002.

*Corresponding author: Research Center for Advanced Manufacturing, Southern Methodist University, 1500 International Parkway, Suite 100, Richardson, TX 75081, USA.

process. In the DCEN period, the concentrated arc can deeply penetrate the workpiece, while the DCEP arc can remove the oxide film on the workpiece surface due to the bombardment from the heavy ions travelling to the workpiece. This process is called the cathodic cleaning action from a DCEP arc. VPPAW is an ideal arc welding process for aluminium alloys because it features gas pore-free and a full-penetrated weld bead in a single pass of thick sections ranging from 3 to 25 mm. Compared with other welding processes, VPPAW can generate a higher welding quality and a higher productivity at a relatively lower cost. VPPAW of aluminium alloys in the keyhole mode has been used successfully in production [1–4]. This attractive feature is attributed mainly to a full-penetrated keyhole-mode welding process. However, keyhole collapse and burn-through may occur during a welding process if disturbances such as abruptly varying thermal conditions exist, especially when welding a thick workpiece. How to control the stability of the weld penetration to achieve a satisfactory weld is still a challenge. One effective approach is to monitor the keyhole welding pool.

The present sensing techniques for the stability of the welding pool or the weld penetration in the keyhole plasma arc welding (PAW) can be divided into two classes according to the relative spatial location of the sensor and the workpiece: sensing from the back side of the workpiece and sensing from the front side of the workpiece. Two difficult problems exist with the front-side sensing of the keyhole welding pool in PAW: the inaccessibility of the welding pool because of the limited torch stand-off distance and the interference of the arc radiation. The PAW technology in the one-keyhole-per-pulse mode can be fairly well applied to steel. Thus, the arc sound or the arc efflux light from the back side of the workpiece can be used to detect the size of the keyhole. Based on this principle, a full penetration weld bead has been guaranteed in real-time feedback control [5–7]. However, this type of technology is not applicable to the welding of aluminium alloys. Also, detecting the keyhole from the back side of the workpiece is not feasible in some cases. A constant parameter open-loop control of the weld formation has still been used in the VPPAW of aluminium alloys with the keyhole mode.

The front-side sensing of the keyhole welding pool includes mainly three techniques:

1. Arc light sensing. It was found that the presence or absence of a keyhole could be determined by monitoring the ratio of the hydrogen 656 nm line to the argon 696 nm line in the plasma arc column with an optical spectrometer [8]. This ratio decreases abruptly when the keyhole is established, presumably because the hydrogen is flushed out through the keyhole with the plasma jet. By the spectroscopic study of the plasma arc, the information on the keyhole formation

can be extracted in the plasma arc welding as well [9]. However, neither can the keyhole size be detected precisely nor can the cutting mode be distinguished from the keyhole mode by this sensing technique.

2. Sound sensing. Sound sensing has been investigated in the PAW process. For example, the sound signal reflects the appearance and disappearance of the keyhole in the PAW of aluminium with direct current reverse polarity (DCRP). The sound signal could be used to control the start or stop of the welding carriage [10]. A workpiece with a variable thickness is used to generate the no-keyhole mode, transition mode and keyhole mode welding pool in the PAW process. It is found that the no-keyhole mode, transition mode and keyhole mode can be identified by the sound signal [11, 12]. However, it remains in question whether the sound signal can be used to identify the cutting mode from the no-keyhole mode and keyhole mode.
3. Image sensing. The many advantages of image sensing include the following: it is intuitive, provides an abundance of information, has an absence of electromagnetic interference and is not intrusive.

In recent years, welding researchers have focused on using machine vision to sense the welding pool for controlling the full penetration in GTAW and gas metal arc welding (GMAW) [13–18]. The arc light filtering solution is investigated through coaxial viewing of the welding pool in GTAW [19]. This approach is based on the principle that the diffuse reflection of the arc light from the welding pool surface is weaker than that reflection from the surrounding area. Thus, the welding pool produces a dark area in the image while the solid part of the workpiece appears as a bright area. Some researchers use a high-shutter-speed camera along with a pulsed-nitrogen laser to overcome the arc light interference in the GTAW of stainless steel [20–22]. With this approach, a clear image of the welding pool is captured and the welding pool boundary is calculated in real-time using a developed image-processing algorithm. The rear angles and the length of the welding pool characterize the geometrical appearance of the welding pool. In the occurrence of full penetration, the back-weld bead width could be related to the geometrical features of the front side of the welding pool. An infrared thermograph is also extensively investigated [23–25]. The researchers found that the interference of the bright arc light could be prevented, and the depth of the joint penetration could be determined using the characteristics of the temperature profiles of steel in the GTAW. The instantaneous decrease of the welding current is used to weaken the intensity of the arc light in order to capture a clear welding pool image during the welding process [26]. However, this approach may not be acceptable due to the poor weld bead that occurs in some cases, e.g. in the VPPAW of aluminium alloys using the

keyhole mode. It is found that the information obtained from the visible keyhole image can be used to successfully control the welding pool stability or the weld formation in VPPAW [27, 28]. However, the field-of-view of the keyhole from the front side of the workpiece is very limited because the stand-off distance of the welding torch is only about 5.0 mm but the diameter of the welding torch is about 50.0 mm. The keyhole image cannot be detected effectively when the keyhole size is out of a specific range. This drawback limits the application of image sensing in VPPAW. Therefore, the key question for front-side image sensing of VPPAW is how to improve the field-of-view of the keyhole welding pool to obtain much more information from it.

This paper focuses on:

- developing a double-image sensor,
- developing an algorithm for image processing,
- establishing the model for the relationship between the keyhole diameter and the geometrical sizes of the welding pool in the image.

2 DOUBLE-IMAGE SENSING

The keyhole welding pool is shown in Fig. 1. It looks like a hole in the base metal with a larger diameter at the top and a smaller diameter at the bottom. The small diameter

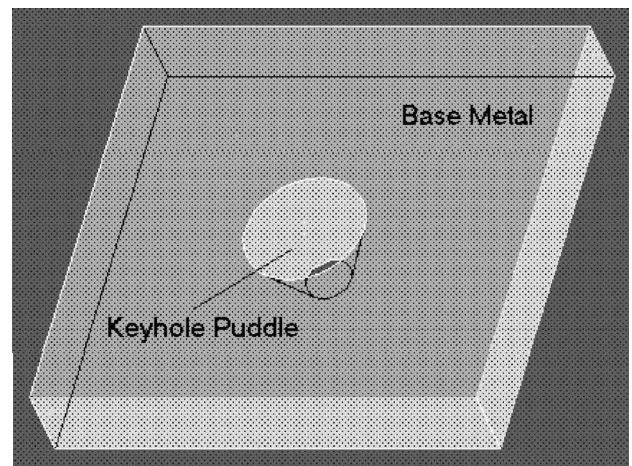


Fig. 1 Schematic diagram of the keyhole weld pool

is called the 'throat' of the keyhole welding pool or the keyhole diameter. In the VPPAW process, the stand-off distance of the welding torch is only about 4.0–5.0 mm, the keyhole diameter is about 2.0–6.0 mm, the thickness of the workpiece is over 4.8 mm and the diameter of the welding torch is about 50.0 mm. Therefore, the field-of-view of the keyhole diameter from the front side of the workpiece is very limited. The limited view remains a big problem even in the case of using a mini-plasma welding torch (the torch diameter is 35.0 mm and the

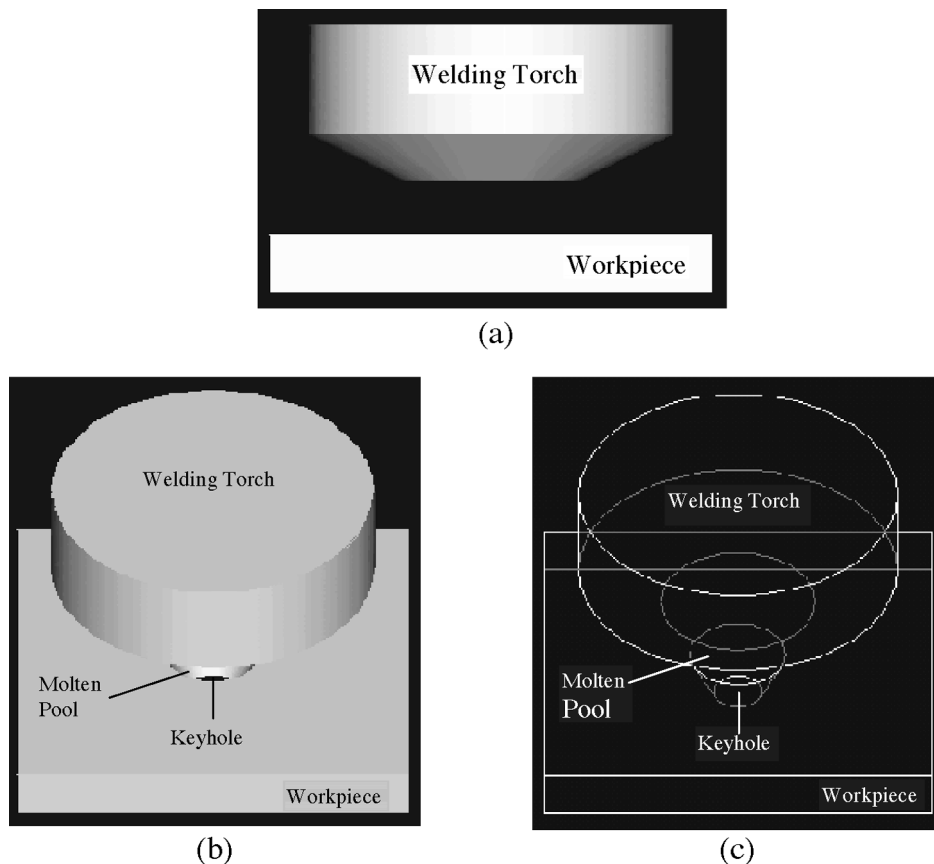


Fig. 2 Views of the welding torch and the workpiece: (a) front view, (b) oblique view, (c) transparent view of (b)

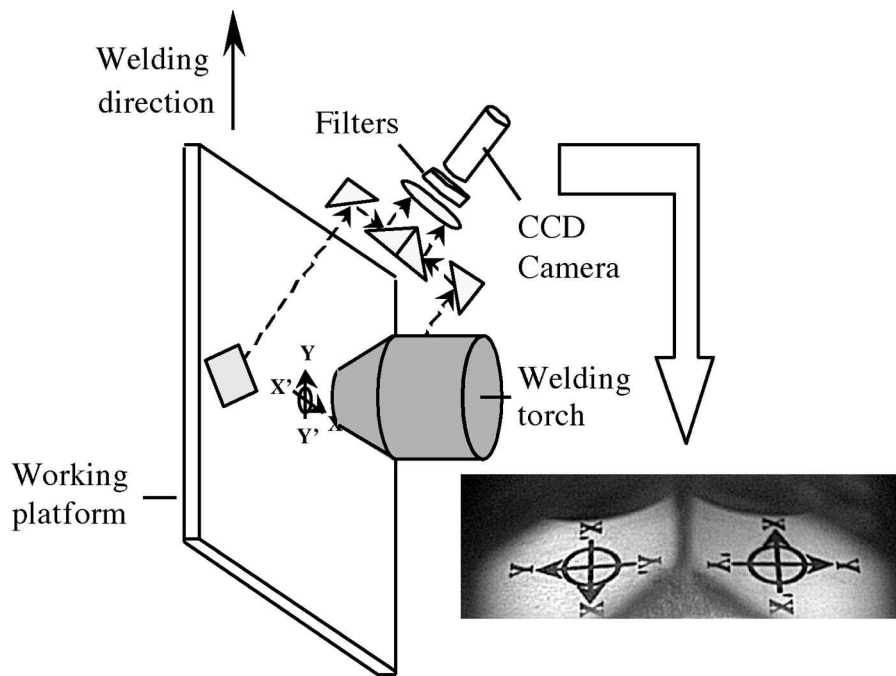


Fig. 3 Schematic diagram of the double-image sensor

nozzle diameter is 14.0 mm). The different views of the keyhole welding pool and the welding torch are shown in Fig. 2. The welding torch and the base metal block most of the view of the 'throat' when trying to acquire the image of the 'throat' of the keyhole welding pool from the front side of the workpiece.

In order to solve this problem, a novel optical system, as shown in Figs 3 and 4, is developed in order to acquire the image of the keyhole welding pool from the left and the right side of the welding torch. The optical system

consists of two flat quartz mirrors that can stand higher temperatures, four right-angled mirrors and a convex lens. The two flat quartz mirrors are fixed vertically to the workpiece surface and have angles of 45° with the welding direction so that the acquired images can be rotated 90° . The reason for using this kind of optical design is that the base metal blocks most of the field-of-view of the keyhole, and only a small portion of the keyhole is visible from the front side of the workpiece. Using a circle to represent the keyhole, the part of



Fig. 4 Photo of the double-image sensor

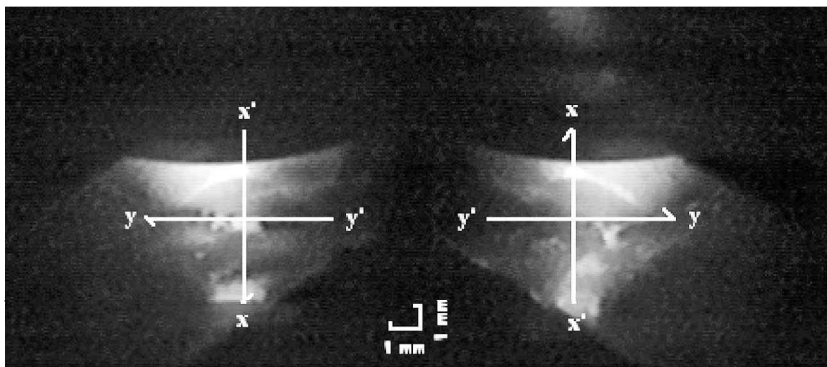


Fig. 5 Front-side image of the keyhole welding pool

the circle located in the YXY' field (more or less depending on the keyhole welding pool size) can only be detected from the left-side mirror, while the part of the circle located in the $YX'Y'$ field can only be detected from the right-side mirror. In previous research works [27, 28], only one image of the keyhole welding pool was used to predict the keyhole diameter, assuming that the shape of the keyhole 'throat' was an ideal circle. With the proposed optical system, the part of the keyhole located in the $YX'Y'$ plane and the part of the keyhole located in the YXY' plane of the keyhole can be acquired in the same frame of the image, providing more information about the keyhole diameter. The keyhole diameter can be determined by the distance $X'X$. The coordinates of the points X' and X can be obtained directly from the image. In this way, a more accurate relationship can be established between the visible keyhole and the keyhole diameter.

The main parameters of arc light filtering are as follows:

- (a) narrow band-pass filter, central wavelength = 670.0 nm, peak transmission = 55 per cent, full width at half maximum = 10.0 nm;
- (b) neutral filters, transmission = 10 per cent.

Figure 5 shows the original images acquired by the developed double-sided image sensor. In the welding process, a high-shutter-speed camera with a pulsed nitrogen laser is used to detect the keyhole diameter directly from the back side of the workpiece. The back-side keyhole diameter data are collected in order to build a neural network model between the visible keyhole and the keyhole diameter. Figure 6 shows the original image of the keyhole welding pool acquired from the back side of the workpiece.

3 KEYHOLE WELDING POOL IMAGE PROCESSING

The $XX'-YY'$ coordinate system in Fig. 3 is a projection of a coordinate system on the surface of the working platform that holds the workpiece to be welded. The projection is fixed in this way: an $XX'-YY'$ coordinate

system is drawn on a paper and fixed on the working platform surface with the original of the coordinate system on the axis of the welding torch. The Y direction coincides with the welding direction. If a workpiece is put on the working platform, the $XX'-YY'$ coordinate system is at the back side of the workpiece. The feature of the acquired image is that the keyhole edge in the YX' plane is clear on the left image and the keyhole edge in the YX plane is clear on the right image. The reason is that the plane of the keyhole 'throat' forms an angle with the top surface or bottom surface of the workpiece surface instead of being absolutely parallel to these two surfaces.

According to the feature of the obtained keyhole image, the purpose of the image processing is to extract the keyhole edge in the $X'Y$ plane on the left image and in the XY plane on the right image. An image-processing algorithm based on image filtering and image enhancement, and an edge-tracing method are developed to detect the edge of the visible keyhole. The image processing steps are:

Step 1. 5×5 median filtering.

Step 2. 45° (for the right image) or 135° (for the left image) direction enhancement.

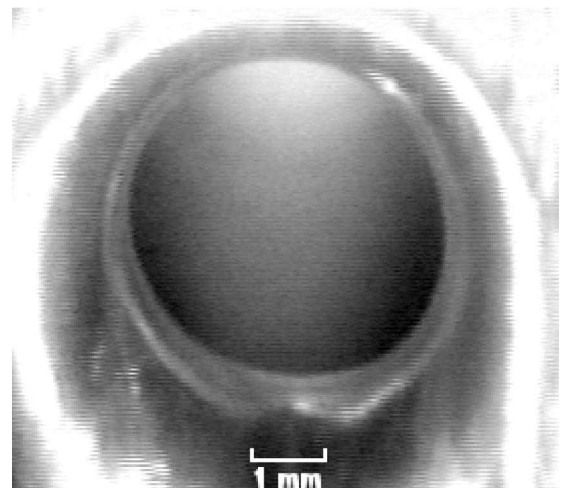


Fig. 6 Back-side image of the keyhole welding pool

$$\begin{array}{cc}
 \begin{bmatrix} 0 & k & k & k & k \\ -k & 0 & k & k & k \\ -k & -k & 0 & k & k \\ -k & -k & -k & 0 & k \\ -k & -k & -k & -k & 0 \end{bmatrix} & \begin{bmatrix} k & k & k & k & 0 \\ k & k & k & 0 & -k \\ k & k & 0 & -k & -k \\ k & 0 & -k & -k & -k \\ 0 & -k & -k & -k & -k \end{bmatrix} \\
 \text{(a)} & \text{(b)}
 \end{array}$$

Fig. 7 Enhancement operators with different directions: (a) 45° , (b) 135°

Step 3. 3×3 minimum filtering, a local statistical characteristic enhancement with a window size of 11×11 .

Step 4. Binary-valued image processing with the threshold of the grey level at 128.

Step 5. Keyhole-edge tracing.

A median (or minimum) filter means that the intensity level of each pixel is replaced by the median (or minimum) of the surrounding pixel grey levels in the filtering window.

A 45° and a 135° direction enhancement means that the intensity level of each pixel is replaced by the convolution of a 45° or a 135° direction enhancement operator and the surrounding pixel grey levels in the image enhancement window. The direction enhancement operators are shown in Fig. 7, where the enhancement factor of K_{en} , the absolute value of the non-zero element of the operator matrix, is set at 0.5.

The local statistical characteristic enhancement is described by the following equations:

$$m_{av}(i, j) = \frac{1}{(2n+1)^2} \sum_{k=i-n}^{i+n} \sum_{l=j-n}^{j+n} f(k, l) \quad (1)$$

where i is the row number and j is the column number of a pixel in the acquired image respectively. The pixel with the coordinate $(0, 0)$ is located on the top-left corner of the image. The symbol m_{av} is the averaged grey level of the pixels included in the enhancement window. The central point of the enhancement window has a coordinate of (i, j) and the size of the enhancement window is $(2n+1) \times (2n+1)$. The symbol $f(k, l)$ is the grey level of the pixel with the coordinate of row k and column l and pixel (k, l) belongs to the enhancement window. Thus

$$g(i, j) = 0, \quad m_{av}(i, j) + K_r[f(i, j) - m_{av}(i, j)] < 0 \quad (2)$$

$$\begin{aligned}
 g(i, j) &= m_{av}(i, j) + K_r[f(i, j) - m_{av}(i, j)], \\
 0 &\leq m_{av}(i, j) + K_r[f(i, j) - m_{av}(i, j)] \leq 255
 \end{aligned} \quad (3)$$

$$g(i, j) = 255, \quad m_{av}(i, j) + K_r[f(i, j) - m_{av}(i, j)] > 255 \quad (4)$$

where $g(i, j)$ is the enhanced grey level of the pixel (i, j) , which is the central point of the enhancement window.

K_r is the ratio of the standard local variance to the original variance with a value greater than 1; K_r is set at 2 in the image processing.

The binary-valued image processing with a threshold grey level of 128 shows that if the grey level of one pixel is equal to or greater than 128, then the pixel's grey level will be set at 255; otherwise, the pixel's grey level will be set at 0. On the binary-valued image, a scanning from the top to the bottom along every column is applied to find the first pixel with a grey level of 255; the pixels are taken as the points on the VK edge. The edge tracing result is shown in Fig. 8a. Four feature points such as A, B, C and D can be detected. Point A is the last point that can be detected along the Y direction on the keyhole edge of the left image. Point B is the intersection point of the XX' axis and the keyhole edge on the left image. Point C is the last point that can be detected along the Y direction on the keyhole edge of the right image. Point D is the intersection point of the XX' axis and the keyhole edge on the right image. In addition, point O_1 and point O_2 are known. The visible keyhole area is defined as the number of pixels included in the quadrilateral ABO_1A' or $DCC'O_2$. Point A' is the vertical projection of point A on the YY' axis. Point C' is the vertical projection of point C on the YY' axis. The VK height is defined as the distance between point B and the origin O_1 or point D and origin O_2 . The VK width is defined as the distance between A' and O_1 or C' and O_2 .

The image processing steps for the back-side image are as follows:

Step 1. 5×5 median filtering.

Step 2. Dividing the image into two symmetric parts, the left part and the right part. The right and left images are enhanced by 0 and 180° direction enhancements respectively. The direction enhancement operators are shown in Fig. 9, where the enhancement factor K_{en} is set at 2.

Step 3. Applying the binary-valued image processing with the threshold of the grey level at 220.

Step 4. On the binary-valued image, scanning from the central to the left side and right side on the lines ranging from 80 to 160. The first pixel with the grey level of 255 along the scanning line is the point on the keyhole edge. Therefore, two points will be found on every scanning line. The distance between the two points is defined as the keyhole diameter of this line. Comparing the length of the detected keyhole diameters, the longest diameter is defined as the visible keyhole diameter. The traced visible keyhole diameter is shown in Fig. 8b.

4 EXPERIMENTAL PROCEDURE

Keyhole welding pools with different keyhole diameters have to be generated. Variations in the size of the keyhole

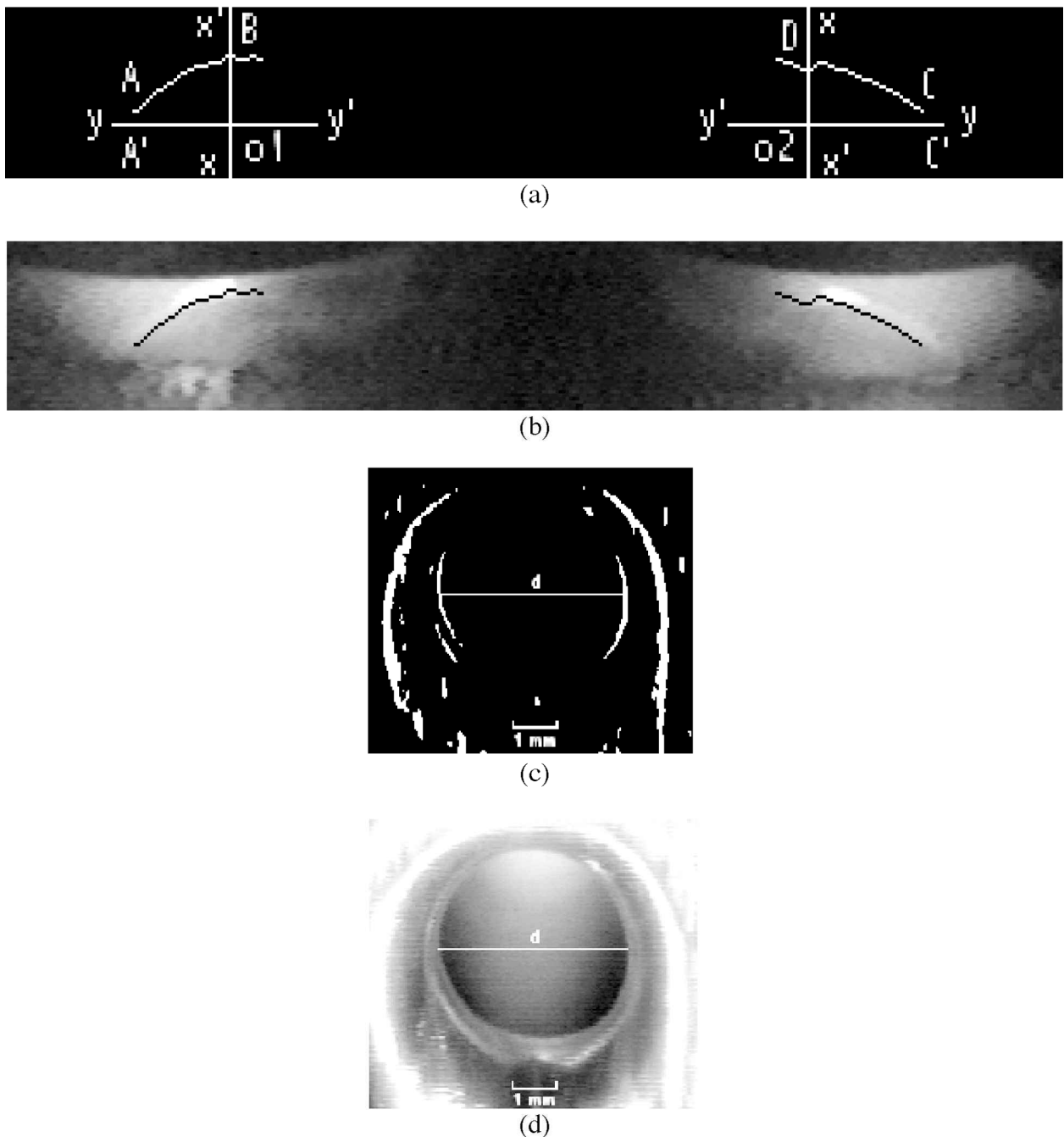


Fig. 8 The edge tracing results, the justification and the definition of the geometric sizes: (a) edge tracing result of the front-side image, (b) edge tracing result and original front-side image, (c) edge tracing result of the back-side image, (d) edge tracing result and original back-side image

diameter can be made by changing some of the welding conditions, such as the welding current, heat sink, wire-feeding speed and welding speed. The following experiments were made for mapping the relationship between the keyhole diameter and the visible geometrical features of the keyhole weld pool image:

1. A regular workpiece with constant welding parameters
2. A varied heat-sink workpiece with constant welding parameters
3. A varied heat-sink workpiece with a variation in the wire-feed speed
4. A varied heat-sink workpiece with a variation in the welding current
5. A varied heat-sink workpiece with variations in both the welding current and the wire-feed speed

The purpose of the variations in the welding current and/or the wire-feed speed is to maintain a continuous welding process and prevent an occurrence of a cutting process. The variations of the welding parameters are

$$\begin{matrix}
 \begin{bmatrix} -k & -k & 0 & k & k \\ -k & -k & 0 & k & k \\ -k & -k & 0 & k & k \\ -k & -k & 0 & k & k \\ -k & -k & 0 & k & k \end{bmatrix} &
 \begin{bmatrix} k & k & 0 & -k & -k \\ k & k & 0 & -k & -k \\ k & k & 0 & -k & -k \\ k & k & 0 & -k & -k \\ k & k & 0 & -k & -k \end{bmatrix} \\
 \text{(a)} & \text{(b)}
 \end{matrix}$$

Fig. 9 Enhancement operators with different directions: (a) 0°, (b) 180°

shown in Table 1. As an example, experiment 4 is executed under the following conditions. The welding current is maintained at an initial value of 100 A until the area with the varied heat sink is reached. Then, the welding current is stepped down to 90 A. When the area with the varied heat sink is passed, the welding current is stepped up again to 100 A. In another example, experiment 6, the initial wire feed speed is maintained at a value of 14 cm/s until the area with the varied heat sink is reached. Then, it is increased to a maximum value of 16 cm/s according to a slope at the middle location of the area with the varied heat sink. Afterwards, it is decreased to the initial value of 14.0 cm/s according to a slope. Every experiment is repeated four times. The first three of the same four experiments are used for model recognition, and the last experiment is used to verify the accuracy of an established model. Every group of parameters associated with image processing is recorded once per second, 20 s after the weld initiation.

The base metal is a 6061 aluminium alloy with a thickness of 4.8 mm. The diameter of the feed wire (ER4043) is 1.2 mm. The constant welding parameters are as follows: the welding speed is 1.6 mm/s, the welding torch stand-off is 5.0 mm, the tungsten setback is 2.5 mm, the orifice diameter is 3.8 mm, the plasma gas flowrate is 3.61/min and the shielding gas flowrate is 9.51/min. Both the plasma gas and the shielding gas are argon. A variable heat sink is made by milling two grooves (40.0 mm

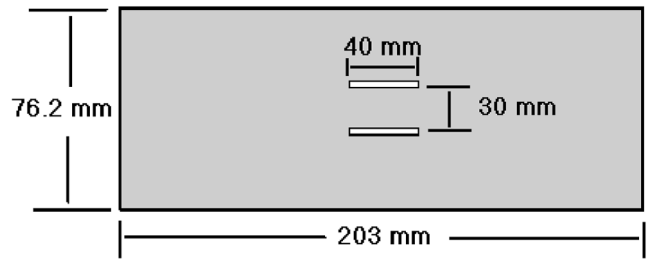


Fig. 10 The schematic diagram of the workpiece with a variable heat sink

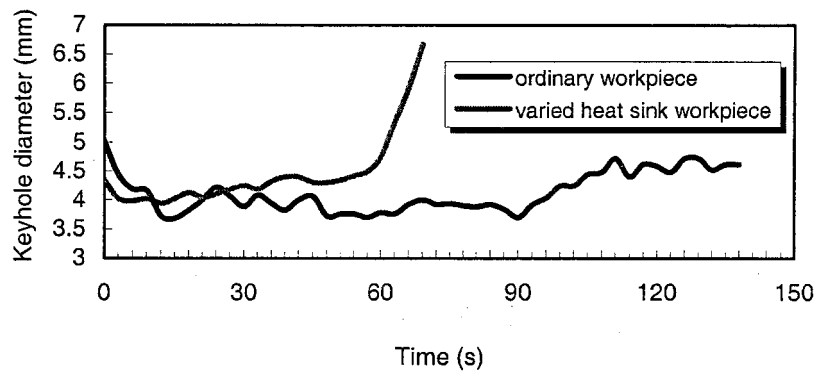
long and 3.0 mm wide) on the workpiece symmetrically, as shown in Fig. 10. The variations of the keyhole sizes with different types of workpiece are shown in Fig. 11. The trends in the change of the real keyhole diameter in the welding process are shown in Fig. 11a. The keyhole diameter has a small increasing trend during the welding process with an ordinary workpiece because of the heat accumulation on the workpiece. A sharp increase in the keyhole diameter occurs at the phase with a varied heat sink condition. The variations of the area, height and width of the visible keyhole obtained by image processing (see Section 3) are shown in Figs 11b, c and d respectively. It can be found that the area, height and width of the visible keyhole can also reflect the corresponding trends in the change of the keyhole diameter. However, none of them can exactly reflect the variation of the keyhole diameter. Therefore, the proposed approach is to predict the keyhole diameter by synthesizing all the information of the visible keyhole obtained from the double-sided images of the keyhole welding pool.

5 ARTIFICIAL NEURAL NETWORK MODELLING FOR KEYHOLE DIAMETER

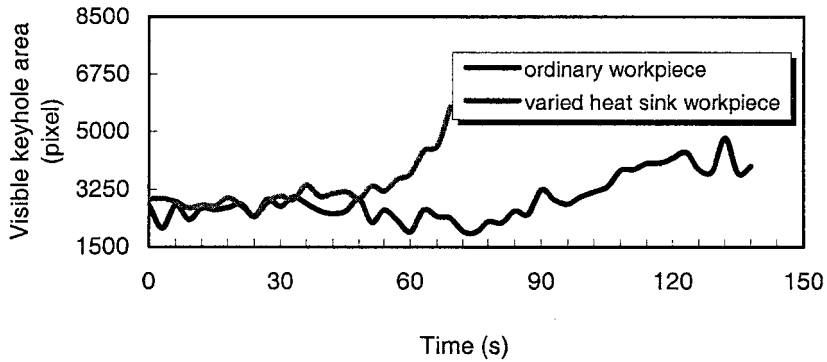
In general, a neural network is an adaptable system that can learn relationships through repeated presentations of data and is capable of generalizing to new, previously unseen data. They provide distinctive features that have a potential application in different areas such as the capacity of learning and adaptation to a problem, massive parallelism and robustness to noise and damage. Neural networks are a set of simple processing elements, each having a small amount of local memory, operating in parallel, whose function is determined by the network structure, connection strengths and the processing performed at computing elements. Figure 12 shows the topology of a simple neural network. On the left are the input units (the input layer), one unit for each item of numerical data. At the right-hand end of the network are output units (the output layer). Between the input and output units, there are the hidden units (the hidden layer) that cannot be directly observed at the input or output of the network. Each processing element (PE) has a set of input links from other units, a set of

Table 1 The welding parameters of a neural network modelling of the keyhole diameter

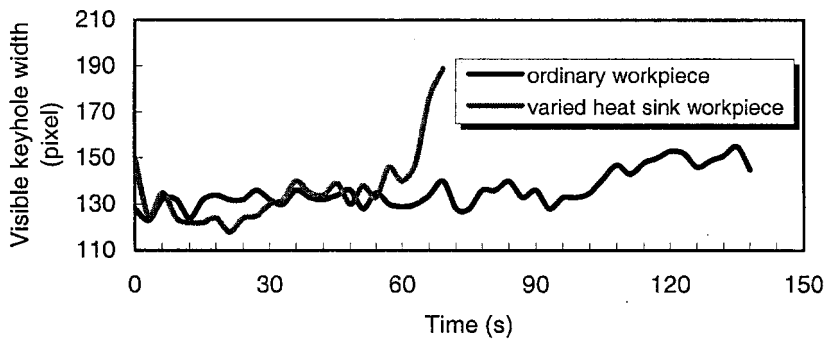
Experiment number	Variable heat sink	Welding current (A)	Wire feeding speed (mm/s)
1	Yes	100	14
2	No	100	15
3	No	100	14
4	Yes	100-90-100	14
5	Yes	100-95-100	14
6	Yes	100	14-16-14
7	Yes	100	14-18-14
8	Yes	100	14-20-14
9	Yes	100-95-100	14-18-14
10	Yes	100-95-100	14-20-14
11	Yes	100-90-100	14-16-14
12	Yes	100-90-100	14-18-14



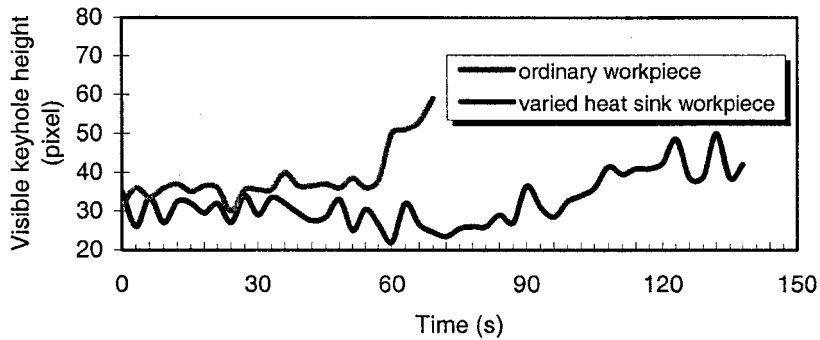
(a) Keyhole diameter versus time



(b) Visible keyhole area versus time



(c) Visible keyhole width versus time



(d) Visible keyhole height versus time

Fig. 11 Variations of the keyhole diameter and the features of the visible keyhole in the VPPAW process with a variable-heat-sink workpiece

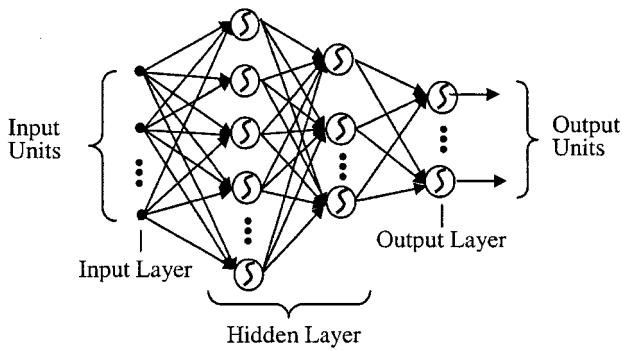


Fig. 12 Schematic diagram of the neural network topology

output links to other units, a current activation level and a means of computing the activation level at the next step in time, given the inputs and link weights as shown in Fig. 13. The computing of the activation level is divided into two components: a linear weighted sum of the unit's input value:

$$in_i = \sum_{k=1}^{jn} w_{k,i} a_k \tag{5}$$

and a non-linear component called the activation function that transforms the weighted sum into the final value that serves as the unit's activation value:

$$a_i = f(in_i) \tag{6}$$

where in_i is weighted sum of the inputs to PE i , a_{jn} is the output of PE jn , $w_{jn,i}$ is the link weight from PE jn to PE i and a_i is the output of PE i .

This activation function is usually represented by the sigmoid function, either in symmetric $[-1, 1]$ or asymmetric $[0, 1]$ form. The sigmoid function is global in the sense that it divides the feature space into two halves, one where the response is approaching 1 and another where it is approaching 0 (-1). Hence it is very efficient for making sweeping cuts in the feature space:

$$f(x) = \frac{1}{1 + e^{-x}} \tag{7}$$

where e is the natural exponent.

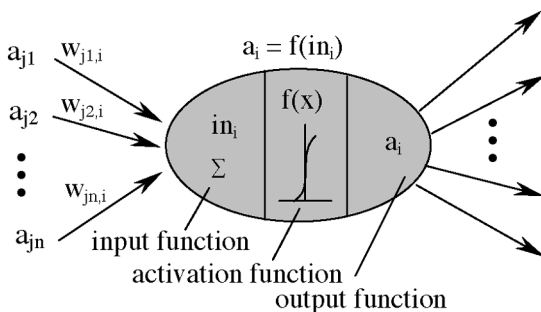


Fig. 13 Schematic diagram of a processing element (PE): in_i , weighted sum of inputs to PE i ; a_i , activation value; $w_{jn,i}$, weight on the link from PE jn to PE i

The most commonly used neural network for practical applications is the multi-layered feed-forward network trained with back propagation (BP). This method learns by calculating the error between the desired and actual output and by propagating this error information back to each node in the network. Then, the back-propagation error is used to drive the learning at each node of the network.

The status of the welding pool has a close relationship with the temperature of the base metal around it. The variation of the temperature of the base metal is continuous and has a very large inertia, especially when the heat conductivity of the base metal is pretty high and the welding speed is slow. VPPAW of aluminium is one of the good examples. Thus, the status of the keyhole welding pool cannot change abruptly. The current status of the keyhole welding pool is related to the foregoing status of the welding pool. Therefore, the foregoing status of the welding pool is important information for predicting its current status. The neural network model consists of three layers: input layer, hidden layer and output layer. There are 16 inputs in the input layer. Fourteen of the 16 inputs are obtained from the acquired image of the welding pool. There are two visible keyhole area values, two visible keyhole height values, two visible keyhole width values and eight coordinates of the four feature points ($x_A, y_A, x_B, y_B, x_C, y_C$ and x_D, y_D). The definitions of the visible keyhole geometrical sizes are shown in Fig. 8a. Two of the 16 inputs are the keyhole diameters in the last status and the status that precedes the last one. There is one output in the output layer: the real keyhole diameter. The unit number, 10, in the hidden layer is determined by trying different unit numbers (6, 8, 10, 12, 14, 16, 18, 20) and comparing the errors of testing and learning. The learning error and testing error are 4.24 and 4.41 per cent respectively. The neural network model is trained with the corresponding software. The comparison between the neural network outputs and the keyhole diameters is shown in Fig. 14.

6 CONCLUSIONS

The image sensing technique is valuable for VPPAW. However, the field-of-view of the keyhole from the front side of the workpiece is very limited. The keyhole image cannot be detected effectively when the keyhole size is out of a specific range. This drawback limited the application of image sensing in VPPAW. A novel image sensor is developed to improve the field-of-view of the keyhole welding pool. Two images of the welding pool from two different directions can be acquired simultaneously in one frame. Thus, much more image information of the keyhole welding pool can be obtained. The geometrical sizes of the visible keyhole on the acquired images can be accurately extracted with the

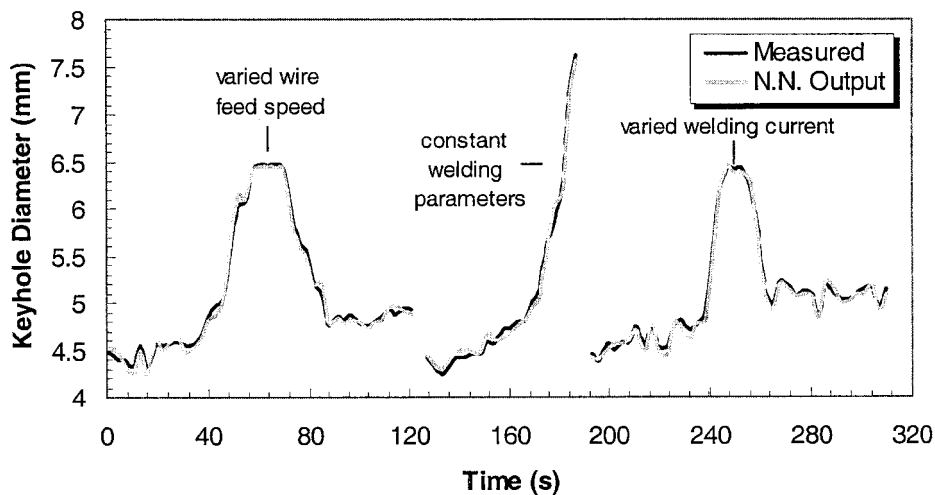


Fig. 14 Testing results of the neural network model

developed image-processing algorithms such as the direction enhancement, the local statistical characteristic enhancement and the edge tracking. It is found that the variation in the size of the visible keyhole has a close relationship with the real diameter of the keyhole. The area, height and width of the visible keyhole can reflect the trend in the change of the real keyhole diameter, but none of them can reflect the trend exactly. An artificial neural network (ANN) model is developed to solve the problem. By training, the model establishes the relationship between the keyhole diameter and the geometrical sizes of the keyhole welding pool obtained from the image. There are 16 inputs in the input layer, 10 PEs in the hidden layer and one output in the output layer. The testing experiment shows that the developed ANN model can effectively and accurately reflect the variation of the real keyhole diameter. By this sensing approach, the real keyhole size of the welding pool can be accurately monitored on-line in VPPAW.

ACKNOWLEDGEMENTS

This work was financially supported by the NSF's Grant DMI-9900011 and by the US Department of Education's Grant P200A80806-98.

REFERENCES

- 1 Nunes, A. C. Variable polarity plasma arc welding on space shuttle external tank. *Weld. J.*, 1984, **63**(4), 27-s–35-s.
- 2 Torres, M. R. Gas contamination effects in variable polarity plasma arc welded aluminum. *Weld. J.*, 1992, **4**, 123-s–130-s.
- 3 Martinez Luis, F. Effect of weld gases on melt zone size in VPPA welding of Al 2219. *Weld. J.*, 1994, **10**, 50-s–55-s.
- 4 Howard, W. A. U.S. contractor for the international space station. *Weld. J.*, 1996, **3**, 35-s–40-s.
- 5 Steffens, H. D. Automatic control for plasma arc welding with constant keyhole. *Weld. J.*, 1972, **6**, 40-s–45-s.
- 6 Metcalfe, J. C. and Quigley, M. B. C. Keyhole stability in plasma arc welding. *Weld. J.*, 1975, **11**, 401-s–404-s.
- 7 Hu, B. X. The study of controlling system of welding quality at all-position by using the arc sound in pulsed plasma arc welding of steel. *Weld. J.*, 1980, **3**, 17–20.
- 8 Martinez, L. F. Front side keyhole detection in aluminum alloys. *Weld. J.*, 1992, **5**, 49-s–52-s.
- 9 Dong, C., Zhu, Y., Zhang, H., Shao, Y. and Wu, L. Study on front side arc light sensing in keyhole mode plasma arc welding. *Jixie Gongcheng Xuebao/Chin. J. Mech. Engng*, March 2001, **37**(3), 30–33.
- 10 Zhang, J. H. and Wang, Q. L. Study on arc sound in TIG and plasma processes. IIW Document 212-610-85, 1985.
- 11 Wang, Y., Chen, Q., Sun, Z., Sun, J. and Wang, H. Sound sensing of the keyhole behaviors in plasma arc welding. *Jixie Gongcheng Xuebao/Chin. J. Mech. Engng*, January 2001, **37**(1), 53–56.
- 12 Wang, Y. W., Chen, Q., Sun, Z. G. and Sun, J. W. Relationship between sound signal and weld pool status in plasma arc welding. *Trans. Nonferrous Metals Society of China*, February 2001, **11**(1), 54–57.
- 13 Nakata, S., Huang, J. and Tsuruha, Y. Visual sensing system for in-process control of arc welding process. *Weld. Int.*, 1988, **12**, 1086–1090.
- 14 Guu, A. C. and Rokhlin, S. I. Computerized radiographic weld penetration control with feedback on weld puddle depression. *Mater. Evaluation*, 1989, **10**, 1204–1210.
- 15 Rokhlin, S. I. and Guu, A. C. Computerized radiographic sensing and control of an arc welding process. *Weld. J.*, 1990, **69**(3), 83-s–95-s.
- 16 Agapakis, J. E. and Bolstad, J. Vision sensing and processing system for monitoring and control of welding and other high luminosity processes. In *International Robots and Vision Automation Conference*, 1991, pp. 23–29.
- 17 Hoffman, T. Real-time imaging for process control. *Advd Mater. and Processes*, 1991, **9**, 37–43.
- 18 Guu, A. C. and Rokhlin, S. I. Arc welding process control using radiographic sensing. *Mater. Evaluation*, 1992, **11**, 1344–1348.

- 19 **Richardson, R. W.** and **Gutow, D. A.** Coaxial arc weld puddle viewing for process monitoring and control. *Weld. J.*, 1984, **63**(3), 43-s–50-s.
- 20 **Kovacevic, R.** and **Zhang, Y. M.** Three-dimensional measurement of weld puddle surface. In International Conference on *Modeling and Control of Welding Processes*, Florida, 1993.
- 21 **Kovacevic, R.** and **Zhang, Y. M.** Vision sensing of 3D weld puddle surface. In 4th International Conference on *Trends in Welding Research*, Gatlinburg, 1995.
- 22 **Kovacevic, R.** and **Zhang, Y. M.** Monitoring of weld penetration based on weld puddle geometrical appearance. *Weld. J.*, 1996, **10**, 317-s–329-s.
- 23 **Nagarajan, S., Chen, W. H.** and **Chin, B. A.** Infrared sensing for adaptive arc welding. *Weld. J.*, 1989, **68**(11), 462-s–466-s.
- 24 **Nagarajan, S., Banerjee, P., Chen, W. H.** and **Chin, B. A.** Weld puddle size and position control using IR sensors. In Proceedings of NSF Design and Manufacturing Systems Conference, Arizona State University, 1990.
- 25 **Chen, W.** and **Chin, B. A.** Monitoring joint penetration using infrared sensing techniques. *Weld. J.*, 1990, **69**(4), 181-s–185-s.
- 26 **Oshima, K.** and **Morita, M.** Sensing and digital control of weld puddle in pulsed MIG welding. *Trans. Japan Weld. Soc.*, 1992, **23**(4), 36–42.
- 27 **Zheng, B., Wang, Q.** and **Kovacevic, R.** Front image sensing of the keyhole weld pool in variable polarity PAW of aluminum alloys. *Trans. ASME, J. Mfg Sci. Engng*, August 1999, **121**.
- 28 **Zheng, B., Wang, H.** and **Kovacevic, R.** Control for weld penetration in VPPAW of aluminum alloys using the front weld pool image signal. *Weld. J./Res. Suppl.*, December 2000, 363s–370s.

Copyright of Proceedings of the Institution of Mechanical Engineers -- Part B -- Engineering Manufacture is the property of Professional Engineering Publishing and its content may not be copied or emailed to multiple sites or posted to a listserv without the copyright holder's express written permission. However, users may print, download, or email articles for individual use.